UNIVERSITÀ DEGLI STUDI DI PADOVA
Department of Land, Environment Agriculture and Forestry

Second Cycle Degree (MSc)
in Forest Science

A comparative study of sensor technologies measuring wind-tree dynamics

Supervisor
PhD. Eng. Luca Marchi
Co-supervisor
Dott. Francesco Zanotto

Submitted by
Piper Desalvo Stone
Student n. 2071422

ACADEMIC YEAR 2024/2025

Index

Acknowledgments

This study was made possible by the University of Padova Department of Land, Environment, Agriculture, and Forestry. The author would like to firstly thank Professor Luca Marchi and Dott. Francesco Zanotto for their guidance. The author would like to extend their gratitude to the private vacation center Pra' delle Torri for access to the trees utilized in this study and to Verde in Quota s.r.l. for their time, equipment, and expertise. Additionally, the author would like to thank Gabriele Dovier for all material and non-material support throughout the entire process.

Abbreviations and Acronyms

DBH	stem diameter at breast height
ξ	damping ratio value of first dampening sway peaks in the pull-and-release test
f_n	average frequency of first dampening sway peaks in the pull-and-release test
FIR	Finite Impulse Response
$H_{1/7}$, $H_{3/7}$, $H_{5/7}$	Relative heights at which the sensor board was mounted to the stem
IMU	Inertial Measurement Unit
IOT	Internet of things
LSB	Least significant bit
MEMS	Micro Electro-Mechanical system
NPSD	Normalized power spectral density
PSD	Power spectral density
RSD	Relative standard deviation
S_1 to S_6	Six sensors mounted of the sensor array
T1 to *T3*	Study trees

Abstract

As climate change intensifies and alters weather patterns, windstorms are expected to increase both in frequency and intensity. Even at present levels, wind is the leading cause of damage to individual trees and entire forests. Many research methods have been developed and many technologies utilized to understand wind-tree dynamics. Yet, there are still no standard practices for monitoring and quantifying wind effects on trees.

This study compares multiple different sensor technologies that have been used in previous studies to record and analyze tree motion in response to wind. Six sensors attached to three living *Pinus spp.* trees were tested through non-destructive pulling tests, pull-and-release tests, and ambient free-sway conditions. The sensors chosen represented a range of sensitivity, resolution, and market cost.

The signals recorded during field tests by each sensor were first processed, then the frequencies and damping ratios calculated and compared. Results showed that the measured response of the tree to excitation is highly dependent on sensor sensitivity and resolution. At low wind speeds, this could result in errors or missing data. Sensor characteristics play an important role in the way study results can be perceived, highlighting the importance of choosing a reliable sensor and utilizing it in a consistent manner. In the future, this study could be replicated to compare other sensors not tested here, or on different tree species with a decurrent growth habit. With further exploration, a standardized set of best practices could be proposed by the scientific community and adopted by practitioners to achieve the best results in understanding wind-tree dynamics.

1 Introduction

The Millenium Ecosystem Assessment published in 2005 by the World Resources Institute classifies four different categories of ecosystem services: provisioning (food, fresh water, fuel, etc.), regulating (climate regulation, water purification, pollination, etc.), cultural (aesthetic, recreational, etc.), and supporting services (soil formation, nutrient cycling, etc.) (MEA, 2005). As is commonly known, trees provide valuable ecosystem services in all four categories. Studies have shown that trees sequester significant amounts of carbon dioxide from the atmosphere (Jo and McPherson, 1995). Especially important in urban areas is the ability of trees to filter particulate matter from the air, which is potentially dangerous to human health. (Nowak et al., 2018). Other ecosystem services provided by trees include reduction of the urban heat island effect, which can decrease energy consumption (McPhearson 2011), and management of stormwater runoff (Kang et al., 2022).

While trees provide numerous benefits, there are also risks associated with tree failure. A falling branch or uprooted tree can cause injury to people and property, and cause thousands of euros of damage. The largest factor contributing to the risk of tree failure is wind (van Haaften et al., 2021). A literature review of studies pertaining to natural disturbances in European forests between the years 1850-2000 found that storms and high winds were responsible for 53% of the total damage in terms of wood volume within that period (Schelhaas et al., 2003). With increasing concentrations of carbon dioxide in the atmosphere and the resulting rise in global temperatures, the intensity and frequency of windstorms is expected to increase, specifically in western Europe (Leckebusch and Ulbrich, 2004). In addition to this, studies have found that increased atmospheric CO_2 can cause trees to grow faster, leading to larger but more fragile trees that could be more susceptible to wind damage (Woolsey, 2022). The combination of these factors highlights the pressing need for accurate and accessible systems to monitor wind effects on trees. By understanding how trees respond to wind, public administrators, forestry companies, arborists, and other stakeholders can make more informed decisions regarding tree management and risk reduction.

Zanotto et al. (2024) compiled an extensive literature review of contemporary methods to monitor and model wind effects on trees. This literature review analyzed over 100 studies starting from 1994 that pertained to wind-tree interactions. Zanotto et al. (2024) classified the studies first based on how the study trees were grown: forest-grown trees, plantation-grown trees, and open-grown trees. Further, the studies included in the literature review were grouped based on whether they focused on conifer tree species, broadleaf tree species, or both. Next, the authors distinguished the studies based on their approach and methodology. The studies included used either dynamic excitation approaches (i.e. field measurements of

tree response to wind, pull and release tests) or static excitation approaches (i.e. destructive or non-destructive pulling tests). A few studies combined both approaches.

To further understand the most studied wind-tree interactions, methodologies, and technologies, and to identify where the largest knowledge gaps may be, the studies in this literature review were grouped based on the objective of the study and the technologies utilized. Some of the objective classifications include testing technologies, model validation, evaluation of growth context, environmental conditions, soil conditions, and sensor calibration. Some of the technologies and instruments utilized in these studies include strain gauges, inclinometers, accelerometers, LiDAR sensors, and load cells. Some studies included in the literature review combined multiple objectives and/or multiple technologies.

Zanotto et al. (2024) found that the most common approach in wind-tree interaction studies over the last 30 years was the dynamic excitation approach of in-situ measurements of tree response to wind. But many limitations and knowledge gaps were found regarding this type of study, including lack of accurate near-ground wind data. The authors also found that although these were the most common type of wind-tree interaction studies, there was no standardized method or procedure shared by the studies. A variety of technologies and research methods were used.

A major limitation of the static excitation approaches (i.e. destructive and non-destructive pulling tests) and the dynamic excitation approach of pull and release tests is that the excitation is artificial. While these methods can be extremely useful for calibrating instruments, measuring root-plate stiffness, and evaluating the elasticity of trunk wood, these artificial tests only provide a momentary view of certain tree properties. They do not give researchers insights into the constantly changing dynamics and responses of the tree the way long-term dynamic monitoring can.

When it came to the different technologies and sensors utilized in wind-tree interaction studies, there is even more variety. Not only were there many different measurement technologies used, such as inclinometers, elastometers, accelerometers, stress gauges, and more, the exact method in which they were used was inconsistent. The height at which the sensors were fixed in the tree, the number of sensors per tree, the technical specifications of each sensor, etc. leads to an incalculable number of possible variations and customizations for each study.

Wind-tree interaction studies have increased within the last five years, as found by Zanotto et al. (2024). Despite this, there is still no standard best practices or consistent methodology. This highlights the need for research combining the various methods and technologies for comparison of strengths and weaknesses of each. This study aims to combine various methodologies and various technologies to compare results and inform methodology

choices in future wind-tree interaction studies. For this study, both aforementioned dynamic excitation approaches (i.e. field measurements of tree response to wind, pull and release tests) and the static excitation approach of non-destructive pulling tests were performed. The technologies utilized in this study were selected among the most common technologies used in wind-tree interaction studies, which included multiple accelerometers and inclinometers with a range of technical specifications and market costs. Two different inertial measurement units (IMU) that combine the technologies of an accelerometer, gyroscope, and magnetometer were used. Elastometers and a tensiometer were also utilized to verify and refine the measurements of the other sensors. Overall, this study combines the most common methodologies and technologies of other wind-tree interaction studies to advance the understanding of benefits and limitations of current practices.

2 Methods and Materials

2.1 Research Site

The data collection for this study took place at a private vacation center, Pra' delle Torri, in Caorle VE, Italia (45°34'05.3"N 12°48'45.9"E) on the days of the 21st and 22nd of October 2024. The environment of the research site was an artificial stand of mixed pine species (predominantly *Pinus nigra, Pinus pinea,* and *Pinus halepensis*) and white poplar (*Populus alba)*. The site of the grove was directly adjacent to a sand beach on the Adriatic Sea. The soil of the site was slightly sandy and compacted due to the frequent foot and car traffic underneath the trees. Ground vegetation was minimal except for a mix of short herbaceous plants. Yearly weather data taken from the nearest Regional Agency for Environmental Protection and Prevention in the Veneto Region (ARPAV) weather station indicated the average temperature of the site is 14.4°C and the total annual precipitation between 2010-2024 is 1091 mm year^{-1}. The weather station that recorded this data was ARPAV station n. 425 located 20 km from the study site (ARPAV Veneto, 2025).

The data collection was conducted on three open-grown trees, henceforth referenced as T1, T2, and T3. The three trees were dispersed throughout the research site, but environmental conditions were consistent for all trees. T1 and T2 were *Pinus nigra* and T3 was *Pinus halepensis*. The trees were chosen based on general health according to visual inspection, height and trunk diameter, trunk shape, and lack of crown interference. Trees with a single, straight trunk and minimal contact with the crowns of neighboring trees were preferred. Specific diameter at breast height (DBH), height, and sensor mounting heights can be found in Table 1.

Table 1. Species, diameter at breast height (DBH), total height, and the height of the mounted sensors during data collection at 1/7, 3/7, and 5/7 of the total height for each of the three study trees.

	T_1	T_2	T_3
Species	*Pinus nigra*	*Pinus nigra*	*Pinus halepensis*
DBH (cm)	23.5	30.5	39.0
Height (m)	16.5	16.5	17.0
$H_{1/7}$ (m)	2.4	2.4	2.4
$H_{3/7}$ (m)	7.0	7.0	7.3
$H_{5/7}$ (m)	11.8	11.8	12.1

On the days of data collection, atmospheric conditions were clear with no precipitation. Airflow data was recorded using two anemometers located within 30 m of the sampling site with a sampling rate of 1 Hz and an accuracy of 0.2 km/h (DynaTree Root and Trunk Testing System, Fakopp Enterprise Bt., Sopron, Hungary). The wind speed and direction were measured and recorded continuously for approximately 8 hours each day throughout the two days of data collection. On data collection days, wind speeds were low but consistent. Measured windspeed data in Table 2 shows the recorded windspeed in m/s in the x- (east-west) and y- (north-south) directions when data was being collected at $H_{1/7}$, $H_{3/7}$, and $H_{5/7}$ of the three study trees.

Table 2. Measured windspeeds in m/s in the x- and y-directions for each tree at each data collection height.

	T_1	T_2	T_3
$H_{1/7}$	0.09, 1.87	0.07, 1.96	0.06, 1.55
$H_{3/7}$	0.08, 1.38	0.05, 1.28	0.01, 0.31
$H_{5/7}$	0.04, 0.82	0.11, 1.20	0.02, 0.37

2.2 Measuring Devices

A wide range of sensors were used in this study, each with varying levels of signal accuracy, sensitivity, cost, and intrinsic function. Two sensor systems were used concurrently: one set to monitor and validate the pull-and-release tests, and one assembly of sensors (henceforth referred to as the *sensor array*) as the principal object of study. The sensor array used to measure the wind-induced response of the study trees consisted of six sensors mounted on an aluminum plate. Small steel bars were attached to the back of the aluminum plate, allowing for ratchet straps to be easily installed and secured to the tree. This setup allowed for efficient installation, adjustment, and removal of the sensor array. The layout also

allowed for all six sensors of principal interest to be mounted and oriented together in a consistent manner.

The sensor array was augmented by various other sensors to verify the data recorded. Two supplemental tiltmeters (Pizzi Instruments, Bagno a Ripoli, Italy) with a range of -15° to +15° were utilized. The first was installed at the base of the tree, approximately 0.1 m above the ground. This tiltmeter remained at the base of the study tree throughout all the tests. The second was installed directly above the sensor board. This second tiltmeter was moved up the study tree with the sensor board as the tests were performed at different heights.

A commercial monitoring system utilized in pulling tests was employed as a reference system for the static excitation tests (e.g. pull-and-release tests and ambient free-sway measurements). This system consisted of two elastometers, three inclinometers, and one load cell (DynaTree Root and Trunk Testing System, Fakopp Enterprise Bt., Sopron, Hungary). The additional inclinometers were placed at ground height around the base of the study tree. The first was installed in the pulling direction (described in section 2.4.1). The second and third additional inclinometers were installed approximately 120° away from the first around the base of the tree. The exact positioning of these sensors was dependent on specific characteristics of the study tree, such as bark thickness and trunk morphology. They were placed in way to attempt the best representation of the individual tree's trunk shape.

Two elastometers were installed on the trunk approximately 1 meter above the ground. They were installed 180° apart, one on the side of the compression wood and one on the side of the tension wood.

Lastly, a tensiometer was utilized in the pulling tests described in section 2.4.1. This sensor was installed between the pulling rope and the base anchor. This sensor measured the force being exerted on the tree during the non-destructive pulling test.

Figure 1. The supplementary sensors used in this study to collect and verify data. This study utilized, in addition to the principal sensor array, two tiltmeters (top left), three inclinometers (top right), two elastometers (bottom left), and a tensiometer (bottom right).

2.3 Sensor Array

The sensor array was comprised of six sensors mounted on the aluminum plate. These are listed with their characteristics in Table 3. Figure 1 shows the exact layout. All sensors on the sensor array were oriented in the same direction. The construction of the sensor array guaranteed that the sensors could all be mounted in the same position and direction on the

tree to allow for consistent measurement. Table 3 is taken directly from a concurrent study utilizing the same array (Zanotto et al., 2025).

Table 3. The characteristics of the six sensors installed on the sensor array.

ID	Company	Model	Sensor Type	Axis Number	Sensitivity	Resolution	Estimated Cost[(1)]
S_1	PCB Piezotronics	393B12	Seismic accelerometer	1	10,000 mV g^{-1}	0.001 g	> 1,000 €
S_2	AD.EL	ASX2000	Accelerometer (MEMS)	3	256,000 LSB/g 400 mV g^{-1}	1.95 µg	500-1,000 €
S_3	Beanair	BeanDevice WiLow HI-INC	Inclinometer	2	0.003°[(2)]	0.001°	500-1,000 €
S_4	Gulf Coast Data Concepts	X2-2	Accelerometer (MEMS)	3	6145 LSB/g	0.0044°[(3)]	< 200 €
S_5	Phidgets	1044_1B	IMU	3+3+3	N/A	0.001 g (76 µg in High-Resolution mode)	< 200 €
S_6	Arduino	MKR IMU Shield	IMU	3+3+3	1000 LSB/g	0.001 g	< 100 €

(1) The estimated cost refers to the whole measurement system of each sensor to acquire the tree vibration, as used in this study.

(2) Repeatability on the full scale

(3) as estimated by (James et al., 2013a; Marchi et al., 2019)

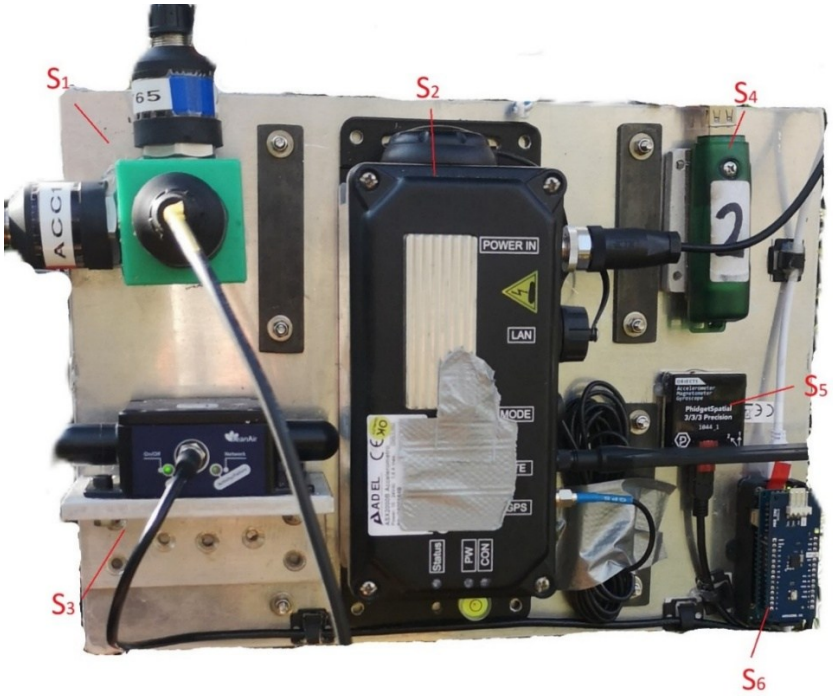

Figure 2. The sensor array used for data collection and measurement comparison. The sensors are labeled according to Table 2.

Figure 3. The sensor array installed in T_1 at $H_{1/7}$.

2.3.1 PCB Piezotronics 393B12 Seismic Accelerometer (S_1)

The first sensor of the sensor array is the seismic accelerometer, model 393B12, by PCB Piezotronics (393B12, PCB Piezotronics, Depew, New York, USA). This sensor, due to its extremely high sensitivity, is typically used for structural engineering and monitoring applications, but was used by Giachetti et al. (2022) and Zanotto et al. (2024a) for an operational modal analysis of living trees. The 393B12 has the capability "to take low frequency measurements to micro-g levels" (PCB Piezotronics). The 393B12 is often used to monitor seismic activity such as earthquakes and tremors, and is used in structure and bridge monitoring to detect vibrations at extremely low frequencies, such as those made by automobiles, trains, and even foot traffic. This sensor has one of the highest sensitivities available on the commercial market, at 10,000 mV g^{-1}. The PCB 393B12 can measure accelerations with a resolution of 0.001 g, with a measurement range of ± 0.5 g, if provided with a 0 to 10 V amplitude. The frequency range of this accelerometer is 0.15 to 1,000 Hz. In this study, the sampling frequency was set to 100 Hz. Given the ability to detect such low frequency vibrations, the 393B12 is capable of providing reliable results of wind-induced tree response even at low wind speeds.

Three 393B12 sensors were installed orthogonally to each other on the sensor board. This allowed for data collection in three directions (*x-, y-,* and *z*-axis). The acceleration signal was captured using a specific Data Acquisition Module (DAQ) and transferred from the module to a laptop (NI-9234 C Series, National Instruments, Austin, Texas, USA), a chassis control (cDAQ-9174, National Instruments, Austin, Texas, USA), and dedicated software to collect the raw acceleration data. The PCB 393B12 inherently blocks constant (DC) signals that do not respond to static forces. The accelerometer naturally removes DC components, including steady-state accelerations. Given the high sensitivity and accuracy of this sensor, it was used as a reference system for the other sensors of the sensor array in the comparative analysis.

2.3.2 AD.EL ASX2000 Accelerometer (S_2)

The ASX2000 accelerometer by AD.EL (ASX2000, AD.EL, Martellago, Italy) is a triaxial micro-electromechanical accelerometer based on the ADXL355BEZ by Mouser Electronics (ADXL355BEZ, Mouser Electronics, Mansfield, Texas, USA). Primarily used in robotics, structural health monitoring, and seismic imaging, the ASX2000 has not been used in tree dynamics research before this study. This sensor has a resolution of less than 0.001 g, in the range ± 2 g, and a sample frequency range of 250 to 1000 Hz. A finite impulse response (FIR) filter is automatically applied with a cut-off frequency of 80 Hz. In this study, the sampling frequency was set to 250 Hz. The data is transferred wirelessly through a 4G modem, and the sensor configuration, real-time monitoring, and data transfer can be managed remotely. The sensor

data is also stored in an SD card that is accessible remotely through a Wi-Fi connection. Data was acquired via a proprietary software developed by the same producer. The software exploits a custom API accessible via a traditional network.

2.3.3 BeanAir BeanDevice WiLow HI-INC Inclinometer (S_3)

The BeanDevice WiLow HI-INC 30B (BeanDevice WiLow HI-INC, BeanAir, Berlin, Germany) is a wireless Internet of Things (IoT) biaxial inclinometer based on micro-electromechanical (MEMS) technology. The BeanDevice has been predominantly used for structural monitoring, but was used by Marchi et al. (2021, 2024a, 2024b) in tree dynamics research. The sensor accuracy is 0.020° and a resolution of 0.001°. The sampling frequency was set to 100 Hz for this study. This inclinometer has a built-in datalogger which allows for wireless transmission of data and real-time measurements. Data was acquired via the proprietary software Beanscape Wilow Basic version 3.0.2.24 using a traditional 2.4 MHz wireless transmission protocol IEEE 802.11n.

2.3.4 Gulf Coast Data Concepts X2-2 Accelerometer (MEMS) (S_4)

The X2-2 sensor (X2-2, Gulf Coast Data Concepts, Waveland, Mississippi, USA) is a triaxial MEMS accelerometer. This sensor has been used in previous studies to monitor the wind-induced response of trees, including James et al. (2013a, 2013b) and Marchi et al. (2019, 2021, 2022, 2024a, 2024b). The X2-2 has a resolution of 0.0044° when run in the ±1.25 g range, as calculated by James et al. (2013) and Marchi et al. (2019). The sampling frequency range for this sensor is between 8 and 512 Hz. For this study, the sampling frequency was set to 128 Hz. This sensor also includes a built-in datalogger that stores the data on and SD card. The sensor output is oversampled and processed through a Finite Impulse Response (FIR) filter.

2.3.5 Phidgets 1044_1B IMU (S_5)

The PhidgetSpatial Precision 3/3/3 High Resolution 1044-1B inertial measurement unit (IMU) (1044-1B, Phidgets, Inc., Calgary, Canada) is a multifunctional sensor. This IMU combines a 3-axis accelerometer, a 3-axis magnetometer, and a 3-axis gyroscope. The accelerometer has a resolution of 976 µg, but also utilizes a high-resolution mode. When the Phidgets sensor measures an acceleration value of less than 2 g, the high-resolution mode is activated automatically and the resolution is increased to 76 µg. The sampling frequency ranges from 1 to 250 Hz, and was set to 100 Hz for this study. The magnetometer has a resolution of 1.5 mG, and the gyroscope has a resolution of 0.0031°/s (Phidgets Inc.). The signal data is captured and archived with a Raspberry Pi 4 board (Raspberry Pi 4, Raspberry Pi Foundation, Cambridge, UK). A custom code was designed using Python language (Python 3.11.4, Python Software

Foundation, Wilmington, DE, USA) that automatically started data acquisition as the Raspberry Pi was powered up.

Another version of this sensor, without the high-resolution mode, was used by Kamimura et al. (2022, 2024) to study tree dynamics.

2.3.6 Arduino MKR IMU Shield (S_6)

The MKR IMU Shield (MKR IMU Shield, Arduino s.r.l., Monza, Italy) is another IMU sensor with a triaxial 16-bit accelerometer, triaxial 14-bit gyroscope, and triaxial 32-bit geomagnetic sensor. This sensor is based off the Bosch Sensortec BNO055 absolute orientation sensor. When this study was done, the MKR IMU had not yet been used in tree dynamics research.

The MKR IMU Shield has a resolution of 0.001 g. as with many of the other sensors of the sensor array, the sampling frequency was set to 100 Hz. The sensor is mounted on the Arduino MKR WAN 1300 board (MKR WAN 1300, Arduino s.r.l., Monza, Italy) and the signal is captured and stored in an Arduino MKR SD Proto Shield (MKR SD Proto Shield, Arduino s.r.l., Monza, Italy). The MKR IMU utilizes a custom code uploaded into the sensor through the Arduino IDE software (Arduino IDE 2.2.1, Arduino s.r.l., Monza, Italy). The code was designed to automatically start data acquisition as the MKR WAN was powered up.

2.4 Data Collection Procedures

The data collection procedure was composed of three tests: non-destructive pulling tests, pull-and-release tests, and ambient sway measurements. The three tests were performed at three different heights along the tree. The heights chosen were at one seventh ($H_{1/7}$), three sevenths ($H_{3/7}$), and five sevenths ($H_{5/7}$) of the total height of the tree. These heights were chosen based on past studies that have shown these ratios correspond to the antinodal points of vibration of the fourth normal mode of a beam fixed at one end (Schindler et al., 2010; Schindler & Mohr, 2018, 2019; Schindler, Schönborn et al., 2013). At these heights, the displacement of the tree during sway is at its maximum, giving the best measurement results. Table 1 shows the various sensor array heights for each study tree. Using a mobile platform, the sensors were installed in the study tree at the first determined height oriented in the pulling direction. After all three types of tests were completed at the first height, the sensor array was moved to the next height. The natural inclination of the trunk (the offset) was recorded at each height to normalize the sensor data. In total, we collected data from 27 non-destructive pulling tests, 27 pull-and-release tests, and recorded over two hours of ambient sway data.

2.4.1 Non-Destructive Pulling Tests

Three non-destructive pulling tests were performed for each study tree at each of the three determined data collection heights. These tests mainly served to provide reference data to assure proper sensor functioning during the pull-and-release tests. From the data recorded during the non-destructive pulling tests, the modulus of elasticity (*MOE*) was calculated according to the process described by Krišāns et al. (2022). These values were used as a simple confirmation that the health status of the trunk wood of each of the three study trees was relatively similar and exhibited relatively equal elastic properties. Combining this information with the visual tree assessment done before testing, we are confident that the three trees used for data collection were not compromised by any major internal defects that could corrupt our results.

The non-destructive pulling tests were performed according to the standard procedure described by Fakopp (Fakopp, 2025). The general principle of the non-destructive pulling test is when a slow, consistent pulling force is applied to the tree until a predetermined change in inclination is recorded. The force required to exert this change in inclination is measured with a tensiometer.

The first step in performing the pulling test is determining the height of the pulling rope. In our study, the pulling rope was set as close to exactly 2/3 the total height of the tree as possible, given each study tree's unique canopy structure and branching architecture. Next, a neighboring tree of adequate size and strength was found to be used as the base anchor. These anchor trees were all within 50m of the study tree and were determined via visual assessment to be in relatively good health and of large enough basal diameter to withstand the pulling forces that would be exerted. The azimuth of the pulling direction was taken to later adjust for the prevailing wind direction measured by the anemometer. Using a mobile platform, the pulling rope was installed in the study tree in the direction of the base anchor tree. The distance between the study tree and the base anchor tree was measured. Then, all sensors were installed on the study tree, including the supplementary inclinometers and elastometers installed at the base.

The pulling apparatus was constructed by installing a lever hoist (Robur 1.5-ton, Beta Utensili s.p.a., Sovico, Italy) and a tensiometer between the pulling rope and the base anchor. The lever hoist was turned slowly and consistently, pulling the tree until the inclinometers showed a change in inclination of 0.25°. This limit of 0.25° tilt has been shown to be a threshold in pulling tests where the tree exhibits maximum flexion with no permanent deformation exerted on the trunk (Krišāns et al., 2022). Once 0.25° tilt was reached, the tension on the pulling rope was let out slowly and gently. Limiting the inclination to this level ensured that we did not damage the roots or trunk wood. The sensors concurrently recorded the tension force

and inclination of the tree during the test. The start time of each repetition was recorded to align the data from all the sensors during data processing.

2.4.2 Pull-and-Release Tests

After three non-destructive pulling tests were performed, three pull-and-release tests were completed utilizing most elements of the same setup. The only element of the pulling test configuration that changed was a quick-release carabiner (Quick release 521, Kong, Monte Marenzo, Italy) installed in place of the tensiometer. This mechanism allowed for the instantaneous release of tension on the pulling rope. The sudden loss of tension caused the study tree to sway, and this sway was recorded and analyzed.

The rope was tensioned with the lever hoist in the same method as with the non-destructive pulling tests. When 0.25° of inclination was reached, the quick-release mechanism was pulled and the tension released. The study tree was left to sway until all energy dissipated. When the tree stopped swaying, the pull-and-release test was considered complete. Three pull-and-release tests were performed on each tree at each height. As with the non-destructive pulling tests, the start time of each pull and release test was recorded for data alignment.

Figure 4. The quick-release mechanism installed in place of the tensiometer for the pull-and-release tests.

2.4.3 Ambient Sway Measurements

After three non-destructive pulling tests and three pull-and-release tests, the sensors were left in place in the study tree for a minimum of 20 minutes to record the natural sway of the tree when influenced only by wind. The sensor layout and orientation of the sensor array was kept fixed for this test as it was during the artificial excitation tests. Windspeeds were low on the days of data collection, but they were sufficient to be recorded. After 20 minutes of ambient sway data was recorded, the sensor board was moved to the next height in the study tree and all tests were repeated in the same manner.

2.5 Signal Analysis

2.5.1 Non-Destructive Pulling Test Data

From the non-destructive pulling tests, we recorded concurrent data on the inclination of the tree, the pulling force being applied, and the strain experienced by the tree while being pulled. We converted the strain data to relative displacement and with these values, we followed the calculation process laid out by Krišāns et al. (2022) to calculate the MOE, first finding the basal bending moment (*BBM*) using the force (*F*), height of the pulling rope in the tree (h_{anchor}), and the slope angle of the pulling line (α_{line}) (Eq. 1).

Equation 1

$$BBM = F \times h_{anchor} \times \cos(median(\alpha_{line}))$$

From there, we calculated the MOE by multiplying the BBM by the radius of the tree (*y*) and dividing by the area moment of inertia (*I*) of a circle and the relative displacement (*e*) (Eq. 2).

Equation 2

$$MOE = \frac{BBM \times y}{I \times e}$$

The MOE calculations were made from the force and strain data recorded by the independent sensor system used to verify the data recorded by the sensor array.

2.5.2 Pull-and-Release Test Data

The data recorded during the pull-and-release tests by all six sensors included in the sensor array was processed in the same way. First, the raw samples were resampled to 50 Hz and smoothed using a moving average having a window length of one second. This normalized

the samples that were originally taken at different frequencies due to different sensor properties.

By taking the inverse of the time interval (*dt*) between the sway peaks, we estimated the sway frequency (Eq. 3).

Equation 3

$$f = \frac{1}{dt}$$

Next, the frequencies were averaged by the number of peaks (*n*) (Eq. 4), which in this was the first five. From this, we obtained an average frequency measured by each sensor at each height in each of the three trees.

Equation 4

$$f_n = \frac{\sum f}{n}$$

Following the procedure explained by Moore & Maguire (2004), the approximate damping ratio (ξ_{approx}) was calculated. The equation (Eq. 5) is based on the free vibration decay method and estimates the ratio of two peak displacements (y_n) and (y_{n+m}) measured over *m* cycles of sway.

Equation 5

$$\xi_{approx} = \frac{y_n - y_{n+m}}{2m\pi y_{n+m}}$$

It has been found that this equation consistently over-predicts the damping ratio. Therefore, a correction factor was proposed by Moore & Maguire (2004) to revise the results (Eq. 6). The damping ratio (ξ) was found for each sensor at each height for each study tree.

Equation 6

$$\xi = \xi_{approx} \times exp\left[-1.336(\xi_{approx})^{0.7175}\right]$$

An average sway frequency and average damping ratio was found for each test height ($H_{1/7}$, $H_{3/7}$, and $H_{5/7}$) and the standard deviation calculated for each sensor based on those averages.

2.5.3 Ambient Sway Data

To acquire the ambient sway data, the sensor array was left in the tree at each test height for a minimum of 20 minutes. Due to a technical issue, T_3 was not monitored for the full 20-minute duration, but 13 minutes instead. Despite this, we managed to collect enough data to process and analyze. During the ambient sway data collection, the only force acting on the study trees was wind. Wind speeds were low during ambient sway data collection (see Table 2), but the sensor array captured signal data in both x- (east-west) and y- (north-south) directions.

The ambient sway data was utilized to find the Power Spectral Density (*PSD*) of each recorded signal, which characterizes the frequency content of the data and identifies frequency peaks that repeat periodically (Stoica & Moses, 2005). These identified frequency peaks were compared across all sensors in the sensor array to analyze each sensor's capability of accurately capturing low-magnitude excitation, i.e. ambient sway caused by low-speed wind. To process the signals recorded by the sensor array, the raw data was first filtered with a bandpass filter of fourth order with a low cut-off frequency of 0.2 Hz and a high cut-off frequency of 5 Hz. After, the data from all individual sensors included in the sensor array was resampled to 50 Hz for accurate comparison of the recorded signals. The best straight-fit line was removed using a detrend function and the Power Spectral Density (*PSD*) was formulated using the Hann window of eight segments with 50% overlap. Applying this window function splits the power spectrum into discreet segments and weakens the signal to 0 at the edge of these segments, thereby minimizing the 'spectral leakage' which blurs the boundary of one spectral segment to the next (Panalaran & Sulisetyono, 2024). Next, the PSDs were smoothed using a moving average with a window length of ¼ the sampling frequency, giving us the Normalized Power Spectral Density (*NPSD*) in $[m\ s^{-2}]^2\ Hz^{-1}$.

3 Results

3.1 Non-Destructive Pulling Tests

The MOE calculations were made from the non-destructive pulling test data recorded by the independent sensor system used to verify the data recorded by the sensor array. The independent sensor system was left around ground height (as described in section 2.2) for each round of pulling tests as the sensor array was moved from one height to the next. Although the values in Table 4 are represented as being at the three different sensor array heights ($H_{1/7}$, $H_{3/7}$, and $H_{5/7}$), it is more accurate to say that these values represent three repetitions of the same test on each study tree since the independent sensor system did not change positions. To clarify which MOE value came from which test, they are differentiated by the height of the sensor array. The MOE values and relative standard deviation found for each sensor array height for each tree are found below in Table 4. The average MOE value is also shown.

Table 4. The MOE in Pa calculated for each tree at each sensor height and the relative standard deviation compared to the average MOE and the average standard deviation.

	T_1	T_2	T_3	Average MOE
$H_{1/7}$	8066.47 MPa 4.56%	8574.24 MPa 1.45%	8096.21 MPa 4.21%	
$H_{3/7}$	9633.02 MPa 13.98%	8475.39 MPa 0.28%	7699.56 MPa 8.90%	8451.71 MPa
$H_{5/7}$	9479.48 MPa 12.16%	8589.71 MPa 1.63%	7451.27 MPa 11.84%	

MOE values for wood materials vary significantly based on species-specific wood properties, the moisture content (in this case, 'green' wood; i.e. standing, living trees), and the general health status of the tree. The MOE values found in this study are within a normal range for green wood of *Pinus spp.*, which is typically around 6,000 to 9,000 MPa. For reference, *Advanced Mechanical Engineering Solutions* compiled a list of MOE values (also called Young's Modulus) for different tree species for green wood and for 12% moisture content. Of the six *Pinus* species listed, the range of MOE values for green wood is from 6,800 MPa to 9,600 MPa (*Young's modulus,* n.d.). The MOE values found in this study fall within the accepted range for *Pinus* species. Each MOE value for each tree is within ±14% compared to the average. Even though T_3 is a different *Pinus* species than T_1 and T_2 (T_3 is *Pinus halepensis,* T_1 and T_2 are *Pinus nigra*), the trunk wood exhibits similar elasticity. The three study trees were specifically chosen based on a visual health assessment. The relative similarity of the MOE values verifies the visual assessment and confirms the general consistency of wood elasticity of all three study trees.

These results give more confidence to the results of the pull-and-release tests and ambient sway data. While determining the exact elasticity of the study trees was not the goal of this study, it was a useful step in ensuring reliable data.

3.2 Pull-and-Release Tests

The data collection of the pull-and-release tests was successful across all sensors in each study tree at each test height except for a malfunction of S_3 in T_2 at $H_{5/7}$. The sensors all recorded similar waveforms with almost equal wavelengths up until around 10 seconds of data collection where the measured wavelengths begin to slightly diverge. All sensors except S_3 recorded acceleration values versus time, and these values were used to calculate sway frequency. S_1 and S_2 recorded vastly different amplitudes of acceleration compared to S_4, S_5, and S_6, but the sway frequency was nearly equal. This is because S_1 and S_2 each include a filtering feature that removes signal static. S_1 inherently blocks constant signals that do not respond to static forces, including steady-state accelerations, while S_2 includes an 80 Hz digital filter that removes aliasing noise. S_3 sway frequency was determined by the recorded inclination versus time data, but the waveforms were the same and sway frequencies comparable. Figures 5, 6, and 7 represent the acceleration/inclination versus time data recorded by each sensor in T_1, T_2, and T_3 respectively at each test height. The results of S_3 are separated because of the different measurement units.

The average sway frequency recorded by each sensor of the sensor array in each study tree at $H_{1/7}$, $H_{3/7}$, and $H_{5/7}$ is shown in Figure 8. From this visualization of the data, we see that across all sensors, the sway frequencies recorded in T_1 exhibit much larger variation when you compare across the three test heights for all sensors. More consistent frequencies were recorded in T_2 and T_3, except regarding S_6. In T_2, each sensor except S_2 and S_6 measured equal sway frequencies at $H_{1/7}$ and $H_{3/7}$. In T_3, every sensor except S_6 measured nearly identical sway frequencies at $H_{1/7}$ and $H_{3/7}$. The recorded sway frequencies at $H_{5/7}$ were consistently lower across all sensors in T_2 and T_3. Tables 5, 6, and 7 show the sway frequency values recorded by each sensor at $H_{1/7}$, $H_{3/7}$, and $H_{5/7}$ for T_1, T_2, and T_3 respectively.

Table 5. Calculated sway frequency of each sensor at $H_{1/7}$, $H_{3/7}$, and $H_{5/7}$ for T_1.

T1 Sway Frequency (Hz)	S_1	S_2	S_3	S_4	S_5	S_6
$H_{1/7}$	0.393	0.394	0.399	0.397	0.397	0.398
$H_{3/7}$	0.402	0.389	0.401	0.401	0.401	0.391
$H_{5/7}$	0.385	0.385	0.384	0.384	0.384	0.374

Table 6. Calculated sway frequency of each sensor at $H_{1/7}$, $H_{3/7}$, and $H_{5/7}$ for T_2. S_3 experienced a malfunction and did not record sway data at $H_{5/7}$ for T_2.

T2 Sway Frequency (Hz)	S_1	S_2	S_3	S_4	S_5	S_6
$H_{1/7}$	0.358	0.364	0.364	0.364	0.364	0.368
$H_{3/7}$	0.358	0.359	0.364	0.364	0.364	0.355
$H_{5/7}$	0.355	0.356	***	0.357	0.357	0.348

Table 7. Calculated sway frequency of each sensor at $H_{1/7}$, $H_{3/7}$, and $H_{5/7}$ for T_3.

T3 Sway Frequency (Hz)	S_1	S_2	S_3	S_4	S_5	S_6
$H_{1/7}$	0.382	0.381	0.380	0.380	0.380	0.384
$H_{3/7}$	0.383	0.380	0.380	0.380	0.380	0.375
$H_{5/7}$	0.377	0.376	0.376	0.375	0.375	0.367

The sway frequency classified by test height was averaged across all six sensors of the sensor array. From those averages, the standard deviation of measured frequency by each sensor was calculated. These average frequency values in Hz and the relative standard deviation (*%RSD*) of each sensor are shown in Table 8. The relative standard deviation value for S_3 at $H_{5/7}$ may be skewed because of the missing data from T_2 but was included for consideration.

Table 8. Average sway frequency in Hz classified by test height and the relative standard deviation (*%RSD*) of the measured frequency by each sensor.

	$H_{1/7}$	$H_{3/7}$	$H_{5/7}$
Average Sway Frequency (Hz)	0.380	0.379	0.371
%RSD S_1	0.48	0.33	0.16
%RSD S_2	0.12	0.55	0.16
%RSD S_3	0.08	0.43	1.63(*)
%RSD S_4	0.02	0.40	0.10
%RSD S_5	0.06	0.40	0.10
%RSD S_6	0.59	1.02	1.62

(*) The %RSD of S_3 at $H_{5/7}$ was calculated from the measured sway frequencies of T_1 and T_3. S_3 experienced a malfunction at $H_{5/7}$ in T_2 so the average sway frequency value and %RSD are skewed because of missing data.

For more meaningful comparison, S_1 was chosen as a reference and sway frequencies recorded by the other five sensors were compared using the results from S_1 as a baseline. S_1

has the highest sensitivity out of all sensors in the sensor array. It also has the highest market cost. Because of the higher level of technical specifications and features of S_1 (see Table 3), it was the most logical choice to use as a reference of performance for the other sensors. Table 9 shows the average sway frequency measured by S_1 at $H_{1/7}$, $H_{3/7}$, and $H_{5/7}$ and the relative standard deviation of each of the other five sensors at each test height. The relative standard deviation value for S_3 at $H_{5/7}$ may be skewed because of the missing data from T_2 but was included for consideration.

Table 9. Average sway frequency in Hz as measured by S_1 classified by test height and the relative standard deviation (*%RSD*) of the calculated frequency of each of the other five sensors.

	$H_{1/7}$	**$H_{3/7}$**	**$H_{5/7}$**
S_1 Average Sway Frequency (Hz)	0.378	0.381	0.372
%RSD S_2	0.36	0.87	0.01
%RSD S_3	0.57	0.10	1.47(*)
%RSD S_4	0.47	0.08	0.05
%RSD S_5	0.43	0.08	0.05
%RSD S_6	1.08	1.34	1.77

(*) The %RSD of S_3 at $H_{5/7}$ was calculated from the measured sway frequencies of T_1 and T_3. S_3 experienced a malfunction at $H_{5/7}$ in T_2 so the average sway frequency value and %RSD are skewed because of missing data.

From this analysis we find that S_4 and S_5 most accurately measured sway frequency overall. S_5 was marginally more accurate than S_4 at $H_{1/7}$. S_2 was extremely accurate at $H_{5/7}$ where the movement of the tree was maximal during pull-and-release tests but did not as accurately record sway frequency at $H_{3/7}$. S_3 measured sway frequency well at $H_{3/7}$, but it is difficult to accurately assess the performance of S_3 overall because of the missing data from $H_{5/7}$ of T_2 that skewed the relative standard deviation. S_6 was the least accurate overall across all test heights. S_6 has the lowest sensitivity and market cost of all sensors in the sensor array.

To further compare the performance of the six sensors, the damping ratios were calculated and analyzed. Figure 9 shows the damping ratios calculated for each sensor at each test height in T_1, T_2, and T_3. The damping ratios exhibited extreme variation in T_1 across the three test heights for every sensor. In T_1, the damping ratios of S_2 at $H_{3/7}$ and that of S_6 at $H_{1/7}$ show the largest divergence. The damping ratios found from T_2 and T_3 are much more similar across all sensors. Tables 10, 11, and 12 show the calculated damping ratio for each sensor at each test height for T_1, T_2, and T_3 respectively.

Table 10. Calculated damping ratio of each sensor at $H_{1/7}$, $H_{3/7}$, and $H_{5/7}$ for T_1.

T1 Damping Ratios	S_1	S_2	S_3	S_4	S_5	S_6
$H_{1/7}$	-0.036	-0.032	-0.031	-0.028	-0.027	-0.043
$H_{3/7}$	-0.013	-0.025	-0.012	-0.011	-0.011	-0.011
$H_{5/7}$	-0.025	-0.023	-0.020	-0.018	-0.018	-0.019

Table 11. Calculated damping ratio of each sensor at $H_{1/7}$, $H_{3/7}$, and $H_{5/7}$ for T_2. S_3 experienced a malfunction and did not record inclination data at $H_{5/7}$ for T_2.

T2 Damping Ratios	S_1	S_2	S_3	S_4	S_5	S_6
$H_{1/7}$	-0.012	-0.010	-0.012	-0.011	-0.012	-0.014
$H_{3/7}$	-0.010	-0.009	-0.009	-0.009	-0.009	-0.010
$H_{5/7}$	-0.010	-0.009	***	-0.009	-0.009	-0.010

Table 12. Calculated damping ratio of each sensor at $H_{1/7}$, $H_{3/7}$, and $H_{5/7}$ for T_3.

T3 Damping Ratios	S_1	S_2	S_3	S_4	S_5	S_6
$H_{1/7}$	-0.006	-0.005	-0.008	-0.008	-0.008	-0.007
$H_{3/7}$	-0.005	-0.005	-0.007	-0.007	-0.007	-0.008
$H_{5/7}$	-0.006	-0.006	-0.007	-0.007	-0.007	-0.007

Damping ratios calculated from T_2 and T_3 data were much more informative than those calculated from T_1. In general, the damping ratios from T_2 and T_3 were extremely consistent across all sensors. Based on the larger variation in results of T_1, regarding both sway frequency and damping ratio, there could have been an influence of operator error, resulting in the pull-and-release test procedure not being employed consistently yet since T_1 was the first tree tested.

Similarly to sway frequency, the average damping ratio classified by test height and the relative standard deviation of each sensor was calculated. These results are shown in Table 13. For more meaningful analysis, these calculations were repeated using the S_1 damping ratios as reference. Table 14 shows the average S_1 damping ratios classified by test height and the relative standard deviation of each of the other sensors based on the S_1 values.

Table 13. Average damping ratio classified by test height and the relative standard deviation (*%RSD*) of the calculated damping ratio by each sensor.

	$H_{1/7}$	$H_{3/7}$	$H_{5/7}$
Average Damping Ratio	-0.017	-0.010	-0.012
%RSD S_1	3.28	3.17	7.42
%RSD S_2	8.24	21.67	0.97
%RSD S_3	0.73	4.78	7.15(*)
%RSD S_4	6.74	6.10	5.03
%RSD S_5	6.92	6.11	6.09
%RSD S_6	17.53	1.52	2.04

(*) The %RSD of S_3 at $H_{5/7}$ was calculated from the damping ratios of T_1 and T_3. S_3 experienced a malfunction at $H_{5/7}$ in T_2 so the average damping ratio value and %RSD are skewed because of missing data.

Table 14. Average damping ratio as measured by S_1 classified by test height and the relative standard deviation (*%RSD*) of the calculated damping ratio of each of the other five sensors.

	$H_{1/7}$	$H_{3/7}$	$H_{5/7}$
S_1 Average Damping Ratio	-0.018	-0.009	-0.014
%RSD S_2	9.27	26.01	5.84
%RSD S_3	3.83	1.68	0.24(*)
%RSD S_4	9.57	3.07	11.26
%RSD S_5	9.75	3.08	12.22
%RSD S_6	13.62	1.72	8.55

(*) The %RSD of S_3 at $H_{5/7}$ was calculated from the damping ratios of T_1 and T_3. S_3 experienced a malfunction at $H_{5/7}$ in T_2 so the average damping ratio value and %RSD are skewed because of missing data.

Regarding damping ratios, S_3 showed promising results at $H_{1/7}$ and $H_{3/7}$. The missing data from T_2 skewed the S_3 average damping ratio at $H_{5/7}$ which limits the interpretation of results. S_4 and S_5 show a similar accuracy through damping ratios that they showed through sway frequency. S_4 and S_5 exhibit nearly identical damping ratios for each test height in each tree. The results from S_2 and S_6 are heavily skewed by the outliers: in T_1 at $H_{3/7}$ for S_2, and in T_1 at $H_{1/7}$ for S_6. In T_2 the damping ratios were lower at $H_{1/7}$ across all sensors but most markedly for S_6.

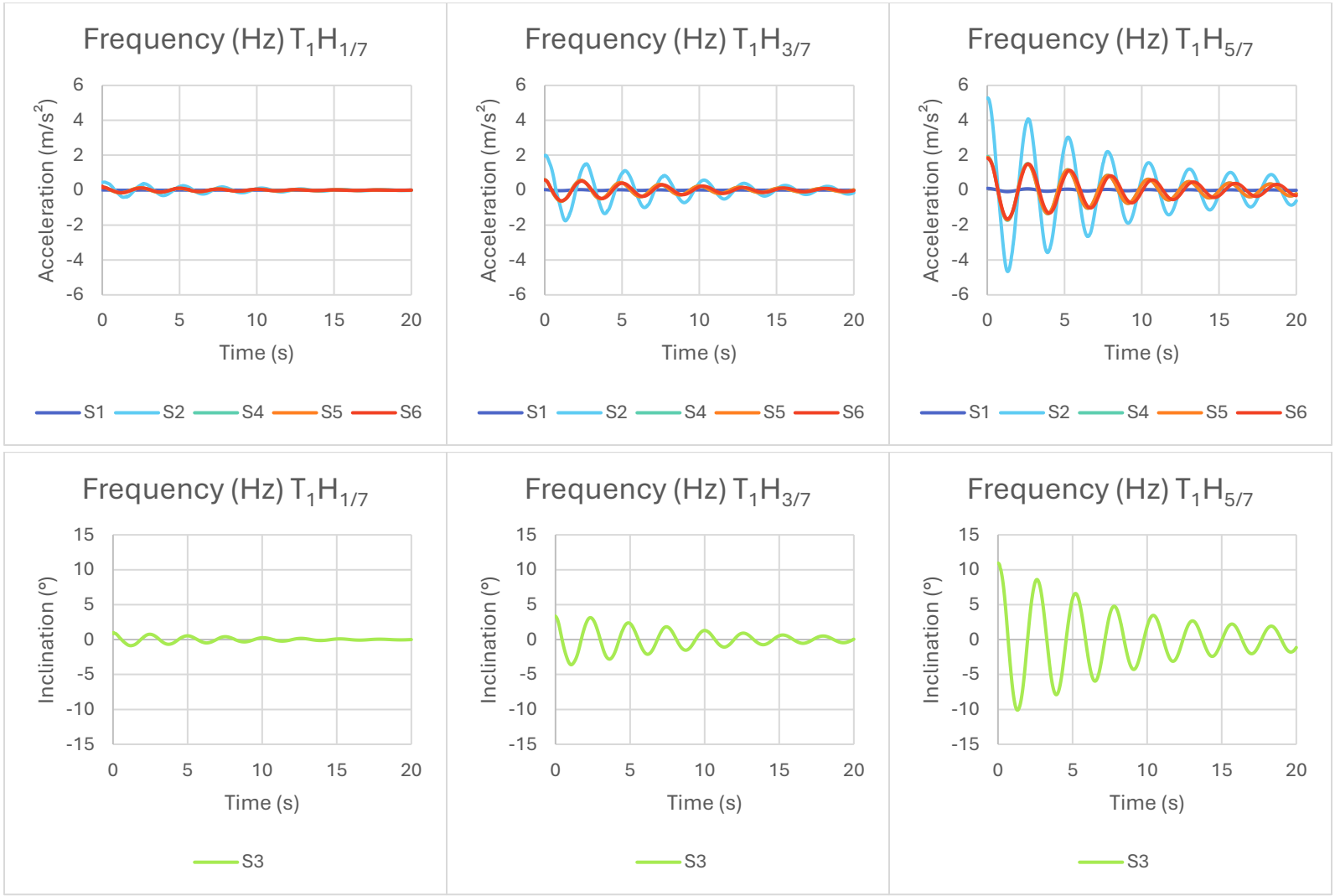

Figure 5. Sway frequency graphs from the pull-and-release tests for each sensor at each testing height in T_1. The top three graphs show all sensors except S_3 with frequency determined by acceleration values in m/s^2 versus time. The bottom three graphs show the sway frequency recorded by S_3, determined by inclination of the tree in degrees versus time.

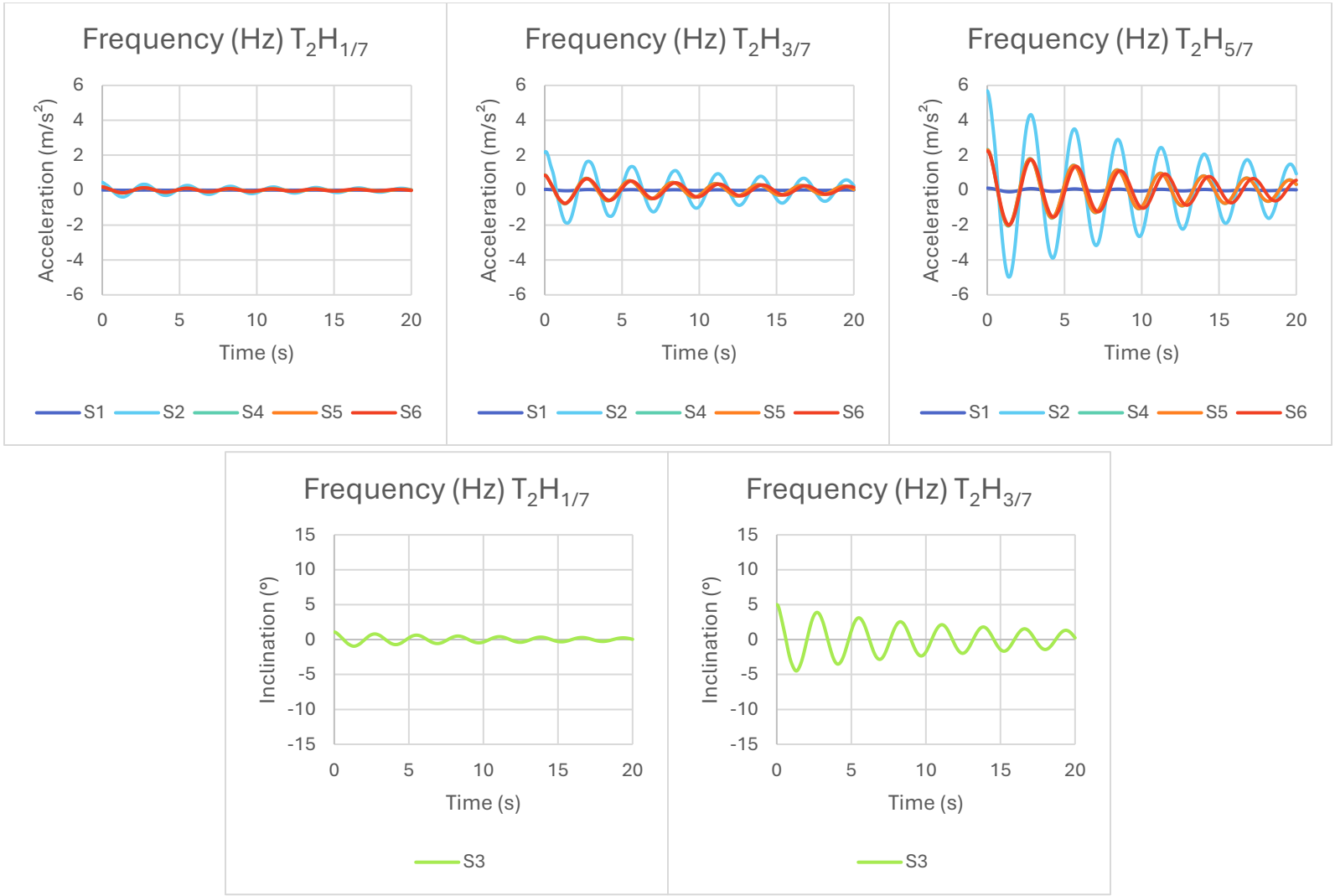

Figure 6. Sway frequency graphs from the pull-and-release tests for each sensor at each testing height in T_2. The top three graphs show all sensors except S_3 with frequency determined by acceleration values in m/s^2 versus time. The bottom two graphs show the sway frequency recorded by S_3, determined by inclination of the tree in degrees versus time. S_3 experienced a malfunction during pull-and-release tests of T_2 at $H_{5/7}$.

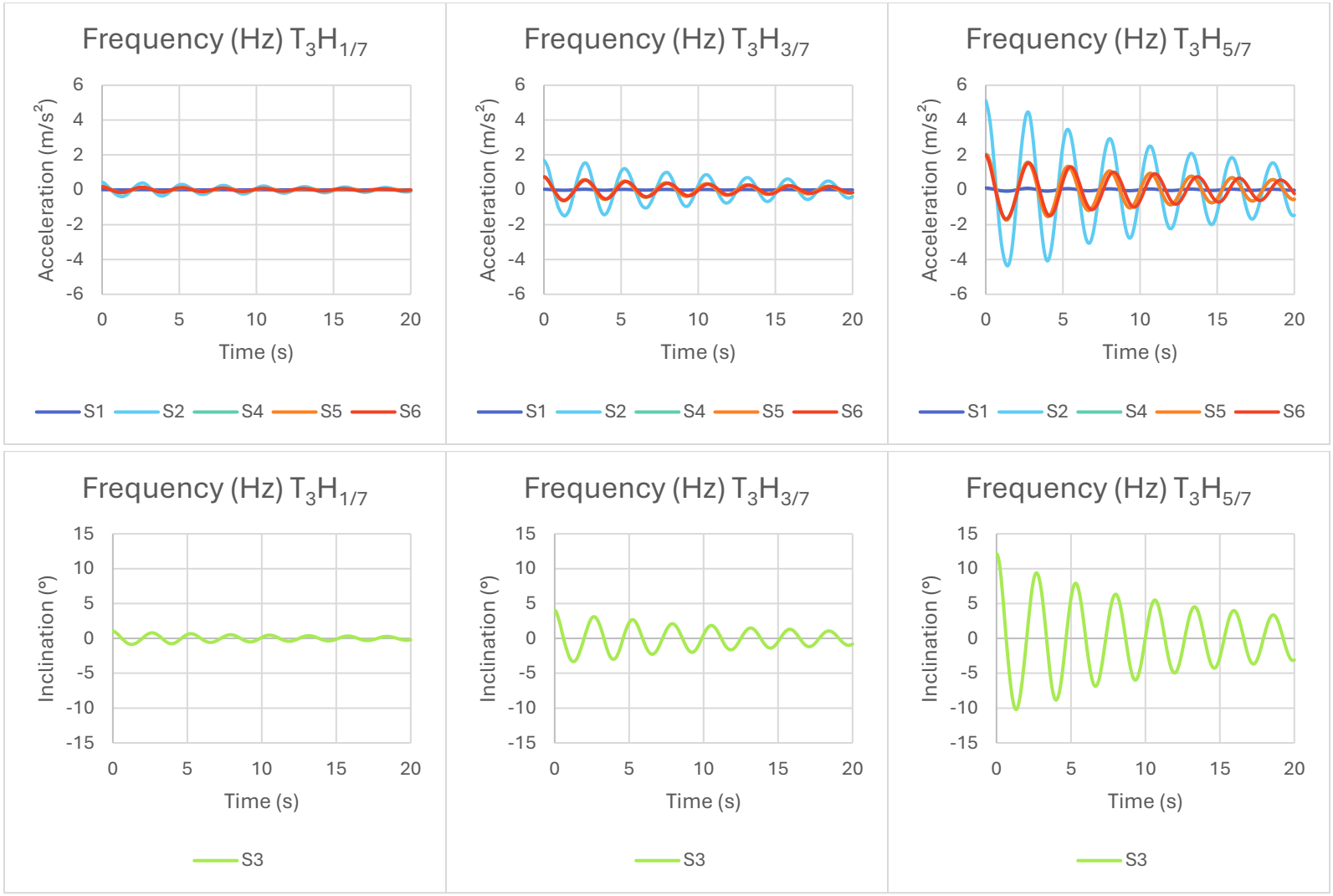

Figure 7. Sway frequency graphs from the pull-and-release tests for each sensor at each testing height in T_3. The top three graphs show all sensors except S_3 with frequency determined by acceleration values in m/s^2 versus time. The bottom three graphs show the sway frequency recorded by S_3, determined by inclination of the tree in degrees versus time.

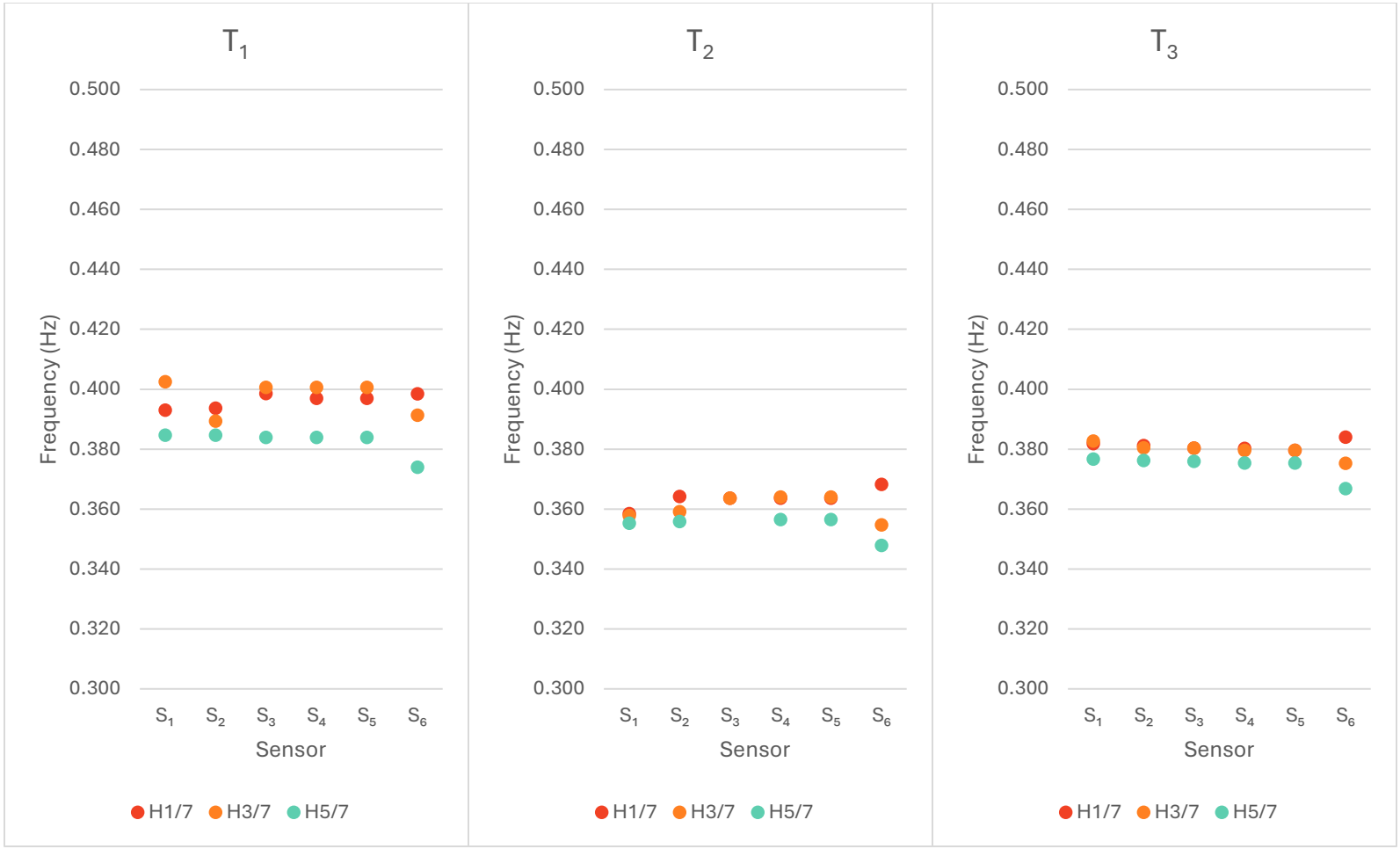

Figure 8. The average sway frequency in Hz measured by each sensor in T_1, T_2, and T_3 at each test height.

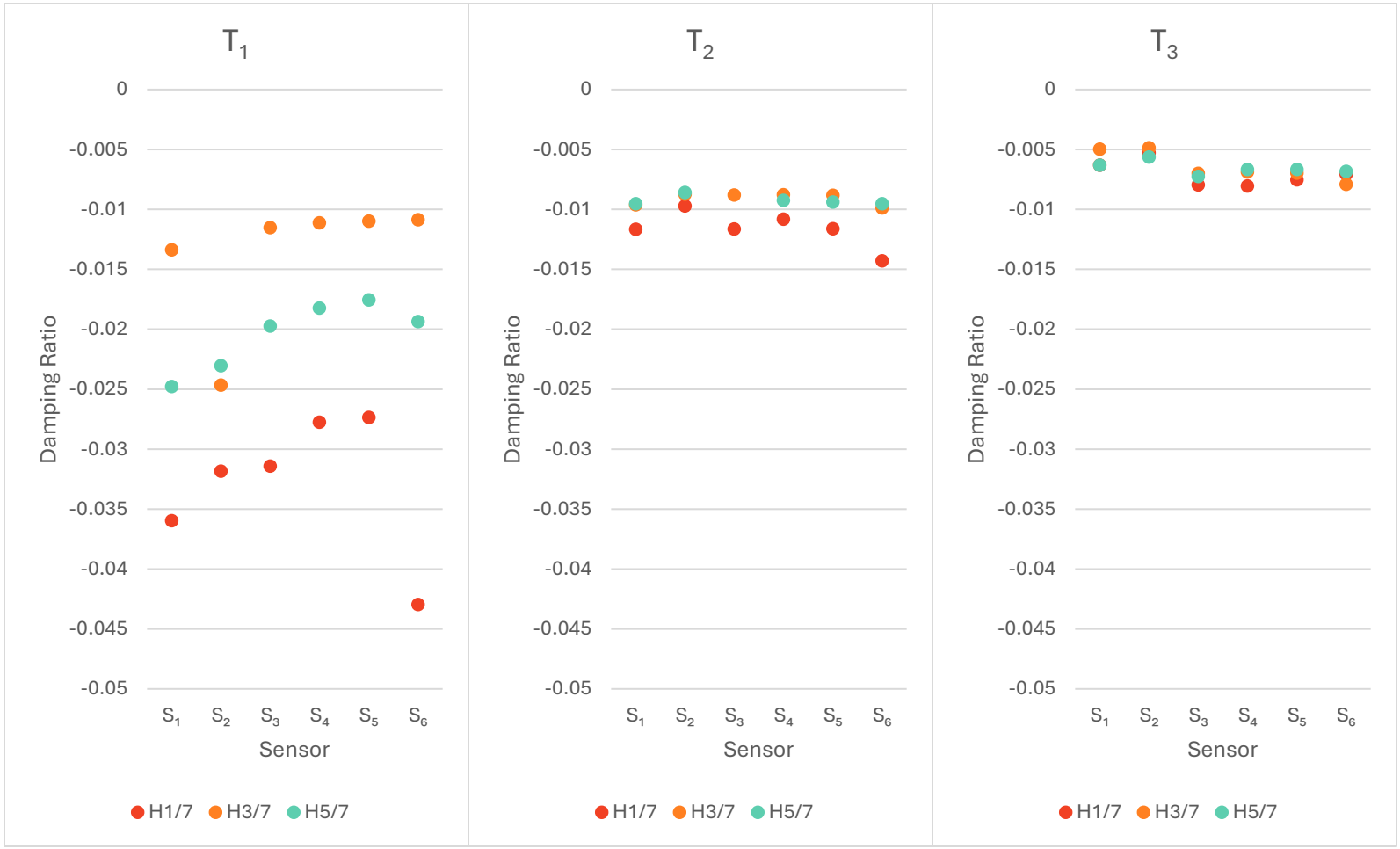

Figure 9. The damping ratio of each sensor in T_1, T_2, and T_3 for each test height.

3.3 Ambient Sway Data

The data recorded during the ambient sway tests was processed to find the Normalized Power Spectral Density (*NPSD*) of each sensor in each study tree at each test height in both the x- (east-west) and y- (north-south) directions. The first sway frequency peak was identified using S_1 as a reference. The frequency peak identified by S_1 was considered the most reliable based on the high sensitivity level of S_1, and each of the other five sensors were compared based on whether they correctly identified the same primary frequency peak identified by S_1. In each NPSD graph, there was one prominent peak ranging from 0.37 Hz to 0.42 Hz. In this analysis, we focused only on this primary frequency peak. The purpose of this NPSD analysis was not to identify every minor sway frequency peak as a function of tree movement, but to calculate the basic rate of sway frequency peak identification by each sensor to compare their efficacy in the field.

A malfunction during ambient sway data collection in T_3 at $H_{5/7}$ lead to unreliable results from all sensors so no frequency peaks could be accurately identified from this data. Figure 10 shows the NPSD of T_1 at $H_{5/7}$ where every sensor accurately identified the primary frequency peak. Figure 11 shows the NPSD of T_3 at $H_{1/7}$ where every sensor except S_4 and S_6 identified the primary frequency peak. In T_2 at all heights, the NPSD of S_2 could not be generated. In T_2 at $H_{5/7}$ the NPSD of S_3 also could not be generated. The NPSD results of T_3 at $H_{5/7}$ were not included in the calculation of the rate of peak identification since the malfunction was consistent across all sensors. In total, the rate of sway frequency peak identification was taken from 16 NPSD graphs, 8 in the x-direction and 8 in the y-direction. The results are shown in Table 15. The rate of peak identification is separated by x- and y-directions and the total rate below.

Table 15. The rate of primary sway frequency peak identification in the x- and y-direction, and the total rate.

	S_1	**S_2**	**S_3**	**S_4**	**S_5**	**S_6**
% X-direction	100	62.5	87.5	37.5	100	37.5
% Y-direction	100	62.5	87.5	75	100	37.5
Total % Peaks Identified	100	62.5	87.5	56.3	100	37.5

S_1 and S_5 identified every primary sway frequency peak in both directions. S_3 identified every peak except where the NPSD could not be generated in T_2 at $H_{5/7}$. S_4 was the only sensor that exhibited a different rate of frequency peak identification between the x- and y-directions. S_6 performed well-below all the other sensors with an average peak identification rate of only 37.5%.

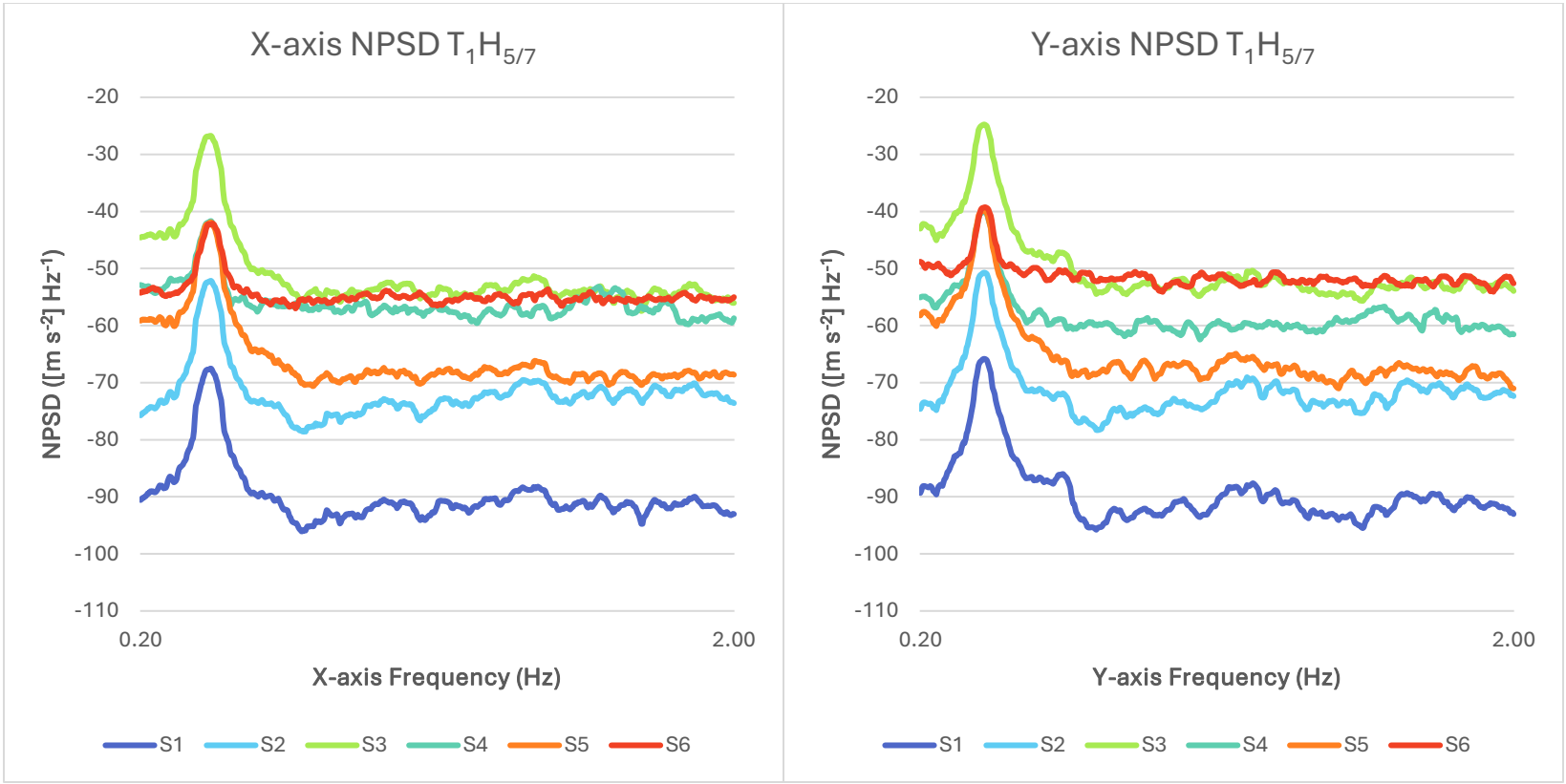

Figure 10. The NPSD of T_1 at $H_{5/7}$ in the x- and y-directions with a sway frequency peak at 0.42 Hz. In this example, every sensor accurately identified the primary frequency peak.

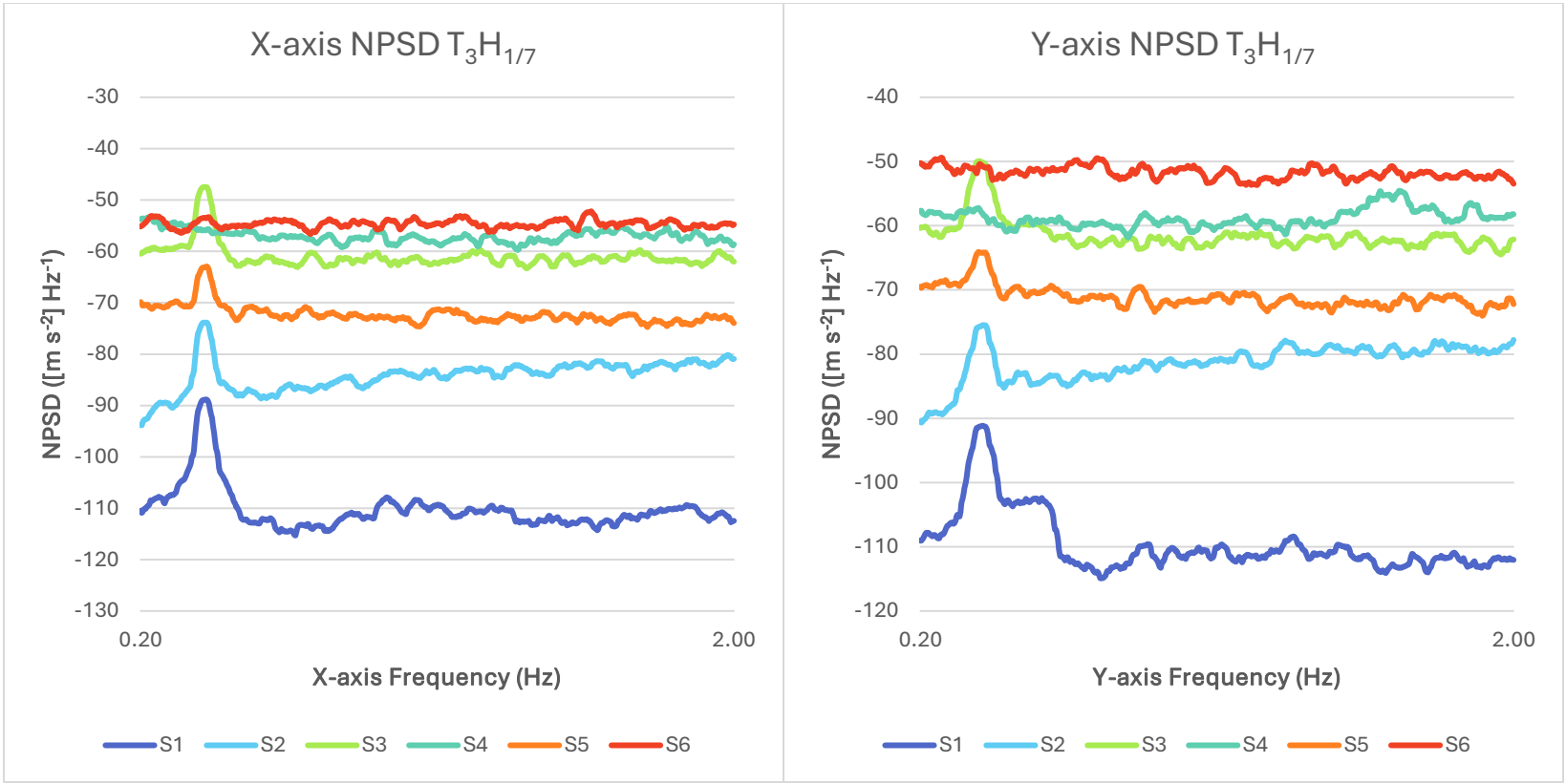

Figure 11. The NPSD of T_3 at $H_{1/7}$ in the x- and y-directions with a sway frequency peak at 0.40 Hz. In this example, S_1, S_2, S_3, and S_5 accurately identified the primary frequency peak. S_4 and S_6 did not accurately identify the primary frequency peak.

4 Discussion

This study design included many different sensor technologies with various specifications, set-up procedures, and data collection modules. While there was a large degree of possible variation and tailoring of the study design, the results of this study managed to highlight the differences in common sensor technologies used in wind-tree dynamics research. Our results were informative despite some sensor errors or data collection malfunctions.

From the results of the pull-and-release tests, we acquired acceleration or inclination data, depending on the sensor, which depicted the waveforms that characterized the swaying motion of the tree. S_1 and S_2 recorded lower absolute values of this data because of inherent filtering software that removes background signals such as steady-state accelerations. Although S_1 and S_2 represented the motion of the tree differently in terms of absolute acceleration values, the waveforms and energy dissipation rendered by these sensors were the same. The measured wavelengths diverged slightly around 10 seconds after initiation but based on the consistency of the waveforms generated by each sensor in the sensor array, we found that every sensor, regardless of measurement units, performed this basic capability well. The only error experienced during this initial data collection stage was the missing data from S_3 in T_2 and $H_{5/7}$. S_3 includes a wireless datalogger, which can be extremely useful for ease of set-up and transportability. But the potential loss of data due to loss of wireless connection, as was the case here, must be taken into consideration when recommending S_3 for use in wind-tree dynamics studies, especially in remote locations where a stable wireless connection is not guaranteed.

From these recorded waveforms, we calculated the sway frequency for every sensor of the sensor array. The sway frequency calculations showed slightly more variation in T_1 but were generally consistent. The sway frequencies calculated from the T_1 data had a maximum range of 0.028 Hz. The sway frequencies calculated from T_2 and T_3 were all within a slightly smaller range. The sway frequencies of T_2 varied by a maximum of 0.020 Hz, and those of T_3 varied by a maximum of 0.017 Hz. The lowest calculated sway frequency came from S_6 in T_2 at $H_{5/7}$ with a value of 0.348 Hz. The highest sway frequency was 0.402 Hz, recorded by S_1 in T_1 at $H_{3/7}$. Given that the range of sway frequency measured across all sensors in all study trees at all test heights was 0.054 Hz with a standard deviation was 0.014 Hz, we found that every sensor included in the sensor array was reliable at this basic level of function.

When using S_1 as a baseline of performance, we found S_4 and S_5 most accurately recorded sway frequency. The relative standard deviation of S_4 and S_5 compared to S_1 when measuring sway frequency was identical for $H_{3/7}$ and $H_{5/7}$, with an RSD of 0.08% and 0.05% respectively. S_5 performed slightly better than S_4 at $H_{1/7}$, with an RSD of 0.43% for S_5 and 0.47% for S_4. S_2 had the lowest RSD of only 0.01% at $H_{5/7}$ but exhibited mediocre performance at $H_{1/7}$

and $H_{3/7}$ with RSDs of 0.36% and 0.87% respectively. S_6 had the highest RSD of sway frequency at all test heights, with 1.08% at $H_{1/7}$, 1.34% at $H_{3/7}$, and 1.77% at $H_{5/7}$.

The next step of the analysis involved calculating the damping ratios from each sensor to compare the way each sensor portrayed the change in motion over time. The results from T_1 exhibited a large degree of variability. In T_1 at $H_{1/7}$, the calculated damping ratio of S_6 was -0.043, which corresponds to a 13.62% RSD for S_6 at $H_{1/7}$ in reference to S_1. Another outlier from T_1, S_2 had a damping ratio of -0.025 at $H_{3/7}$. This damping ratio value was more than double the value recorded by most of the other sensors during this test repetition. At $H_{3/7}$, S_2 had an RSD of 26.01% when compared to the values from S_1. The rest of the sensors recorded relatively consistent damping ratios in T_1 across each test height, but there was still a high level of variation in damping ratios measured by the same sensors at different test heights. For example, even S_1, which is considered the most reliable of all sensors in the sensor array, exhibited a damping ratio range of 0.023 across all tests in T_1. For comparison, the range of S_1 damping ratios calculated from T_2 and T_3 were 0.002 and 0.001 respectively. It is not immediately clear why the pull-and-release test results from T_1 exhibited more variation than those from T_2 or T_3, but considering it was the first tree that these tests were performed on, a possible explanation is simply that the pull-and-release tests were not executed as consistently due to a 'learning curve'.

The damping ratios from T_2 were within a much smaller range than those of T_1 across all sensors. S_6 exhibited the largest divergence at $H_{1/7}$ with a damping ratio of -0.014 compared to an average value of -0.011 for the other sensors at $H_{1/7}$. In T_2, every sensor recorded the same damping ratio at $H_{3/7}$ and $H_{5/7}$, varying between sensors by only 0.001, except S_3 which experienced a malfunction at $H_{5/7}$ of T_2. In T_3, the damping ratio values were extremely consistent. Every sensor exhibited a range of only 0.001 at most between the various test heights. These results give confidence in the pull-and-release test procedure and the sensor array set-up. Even when utilizing various sensors that encompass a wide range of sensitivity, capability, and data collection and storage systems, achieving results of this consistency ensures that the methodology used in this study was sound.

Moving to the results of the ambient sway tests, the discrepancies between the sensors of the sensor array became more apparent. Based on the rates of primary sway frequency peak identification from the NPSD graphs, we can see that while all sensors recorded sway frequency and damping ratio with prevailing regularity, the strength of the frequency signals captured by the individual sensors differed greatly. S_1 identified a very dominant primary sway frequency peak in every tree at every test height in both the x- and y-directions. S_1 even identified many secondary sway frequency peaks, exemplifying this sensor's sensitivity and accuracy. But since the goal of this study was not to thoroughly investigate the NPSD of the motion of the study

trees, we neglected to explore these secondary peaks further since they were not shared by most of the other sensors.

As mentioned before, S_1 exhibited very dominant sway frequency peaks in every ambient sway test. The only other sensor that performed at the level of S_1 was S_5. S_5 had a 100% primary sway frequency peak identification rate. S_3 demonstrated a relatively high level of reliability with 87.5% peak identification. S_2 displayed average performance, while S_4 and S_6 did poorly in this portion of the analysis. S_6 had a lower overall peak identification rate, but S_4 showed inconsistency in peak identification between the x- and y-directions, which was unique to S_4.

When all results from all tests are considered, S_1 and S_5 seem to be the most reliable and accurate choices of sensors for studying wind-tree dynamics. S_1 is a highly professional sensor used in structural engineering and monitoring. The sensitivity and built-in features, such as the constant acceleration filter, set this sensor apart from the other sensors of the sensor array. But this higher level of accuracy is paired with a significantly higher market cost as well. And while the constant signal filter of S_1 can refine the collected data and limit signal noise, this feature should be used with caution so as not to mislead researchers by misrepresenting the absolute acceleration values in wind-tree interactions. This applies to S_2 as well with its 80 Hz finite impulse response filter.

S_5 exhibited the best overall performance when compared to S_1. Because S_5 is a triaxial inertial measurement unit (IMU), this sensor has a wide range of potential measurement and data collection uses. Combining the capabilities of an accelerometer, a gyroscope, and magnetometer expands the range of possibilities for this sensor within wind-tree dynamics studies and in many other fields of research. S_6 is also a triaxial IMU but performed poorly relative to the other sensors in all tests of this study. With a market cost of less than two hundred euros, S_5 could be not only a reliable instrument, but also an accessible instrument for wind-tree dynamics research with financial constraints.

S_3 performed well in all tests similarly to S_5. But the missing data from T_2 at $H_{5/7}$ made it difficult to confidently assess the performance of S_3. Future replications of this study could clarify the performance of S_3 so it could be more accurately compared to the other sensors.

From the results of the pull-and-release tests, S_4 seemed very promising with results similar to those of S_5. But when the ambient sway data and NPSDs were analyzed, S_4 did not reliably represent the distribution of power over the sway frequency spectrum. The results from S_2 across all tests exhibited mediocre performance and S_6 proved to be the least reliable sensor across all tests.

5 Conclusions

This study aimed to meaningfully compare six sensor technologies with potential utility in wind-tree dynamics research. The chosen sensors covered a wide range of functions, sensitivity, and market costs. Some of the sensors had been used in previous wind-tree interaction studies while others had not.

The experimental design included non-destructive pulling tests, pull-and-release tests, and ambient sway data collection. The analysis of each sensor's performance was centered around the recorded sway frequency and calculated damping ratios from the pull-and-release tests. Through each sensor's interpretation of this information, we were able to compare the capabilities and accuracy of the sensor array. By recording and analyzing the ambient sway data, we expanded the evaluation in a meaningful way. Visualizing and assessing the normalized power spectral density (NPSD) of each sensor gave a deeper understanding of not only the absolute motion that each sensor was experiencing, but the intensity of the signals it was recording. The ambient sway and NPSD results created larger distinctions between the sensors.

From these results, we found that every sensor could perform at a basic level the function of recording the acceleration or inclination data needed to find the sway frequency. The quantitative results showed some variation between each sensor, and some sensors stood out as being more accurate than others. The major difference found was in the power spectral analysis, which is a representation of the intensity of the frequency signals that each sensor was reading.

This study was complicated by the various technical specifications of the sensors. The sensitivity of each sensor, which is a major factor in performance, was difficult to quantitatively compare because of the different units of sensitivity between digital and analog accelerometers (i.e. LSB/g versus mV/g). Some technical information could not be found, for example the sensitivity of the Phidgets 1044_1B (S_5). The BeanDevice WiLow HI-INC inclinometer by BeanAir (S_3) added further complications because the sensitivity of the sensor is related to inclination values rather than acceleration values. Various resolution values and other features, such as the constant-signal filters of the PCB Piezotronics 393B12 (S_1) and the AD.EL ASX2000 (S_2), made direct comparison based on technical specifications unconstructive.

Regardless of these difficulties, the experimental design and data analysis was enlightening. Through our tests, we confirmed that the PCB 393B12 (S_1) provided excellent results, which was to be expected based on the high professional level of this instrument, reflected in its market cost. Other than S_1, we found that the Phidgets 1044_1B inertial measurement unit (S_5) exhibited the best performance overall. The market cost of this sensor is significantly lower than the PCB 393B12 which can be a critical factor in experimental design.

This information can help inform future studies of wind-tree dynamics, guiding researchers to understand the benefits and limitations of common sensor technologies.

This study was highly informative about common sensor technologies and their efficacy in wind-tree dynamics research but is by no means exhaustive. There are many potential experiments that could be done to further test the sensors included here. Additionally, new sensor technologies are constantly being developed that could have potential utility in these types of studies. This study is intended as a step in the development of standardized practices for wind-tree interaction research. Replications of this study and expansion of the concepts explored here through new experimental designs will continue the development. There are many possible paths forward to broaden the scope of knowledge, including replicating this study on trees with decurrent growth patterns or even on trees with known damage or decay that makes them more hazardous and therefore a higher priority for intervention. Multi-day ambient sway measurements through higher windspeeds could also illuminate hidden differences between sensor technologies. Ultimately, the goal of this study is to expand our understanding of the best methods to study wind-tree dynamics and to pass this information on to arborists, tree technicians, and other relevant stakeholders so it can be used to make the best management decisions for people and for the trees.

References

Fakopp, (2025). Fakopp pulling test manual [WWW Document]. Fakopp Enterprise Bt. URL https://fakopp.com/docs/products/pullingtest/pullingtest_manual.pdf (accessed 2.1.25).

Giachetti, A., Zini, G., Giambastiani, Y., Bartoli, G., (2022). Field Measurements of Tree Dynamics with Accelerometers. Forests 2022, Vol. 13, Page 1243 13, 1243. https://doi.org/10.3390/F13081243

James, K., Hallam, C., Spencer, C., (2013a). Measuring tilt of tree structural root zones under static and wind loading. Agric For Meteorol 168, 160–167. https://doi.org/10.1016/J.AGRFORMET.2012.09.009

James, K., Hallam, C., Spencer, C., (2013b). Tree stability in winds: Measurements of root plate tilt. Biosyst Eng 115, 324–331. https://doi.org/10.1016/J.BIOSYSTEMSENG.2013.02.010

Jo, H. K., & McPherson, G. E. (1995). Carbon storage and flux in urban residential greenspace. *Journal of Environmental Management*, *45*(2), 109-133.

Kamimura, K., Nanko, K., Matsumoto, A., Ueno, S., Gardiner, B., (2024). Energy transfer during tree movement for different wind conditions and forest configurations. For Ecol Manage 571, 122223. https://doi.org/10.1016/J.FORECO.2024.122223

Kamimura, K., Nanko, K., Matsumoto, A., Ueno, S., Gardiner, J., Gardiner, B., (2022). Tree dynamic response and survival in a category-5 tropical cyclone: The case of super typhoon Trami. Sci Adv 8. https://doi.org/10.1126/SCIADV.ABM7891

Kang, J., Hirabayashi, S., & Shibata, S. (2022). Urban Forest ecosystem services vary with land use and species: A case study of Kyoto City. *Forests*, *13*(1), 67.

Krišāns, O., Čakša, L., Matisons, R., Rust, S., Elferts, D., Seipulis, A., & Jansons, Ā. (2022). A Static Pulling Test Is a Suitable Method for Comparison of the Loading Resistance of Silver Birch (*Betula pendula* Roth.) between Urban and Peri-Urban Forests. *Forests*, *13*(1), 127. https://doi.org/10.3390/f13010127

Leckebusch, G. C., & Ulbrich, U. (2004). On the relationship between cyclones and extreme windstorm events over Europe under climate change. *Global and planetary change*, *44*(1-4), 181-193.

Marchi, L., Costa, M., Grigolato, S., Lingua, E., (2022). Overturning resistance of large diameter Norway spruce (Picea abies (L.) Karst) on sloped conditions. For Ecol Manage 524. https://doi.org/10.1016/J.FORECO.2022.120531

Marchi, L., Costa, M., Locatelli, T., Gardiner, B., Lingua, E., (2024a). Effect of Repeated Pulling Loads on Norway Spruce (Picea Abies (L.) Karst.) Trees. For Ecol Manage 567. https://doi.org/10.1016/j.foreco.2024.122071

Marchi, L., Mologni, O., Byrne, K., Grigolato, S., Roeser, D., (2024b). Cyclic loading effects and stability assessment of trees and stumps used as anchors in cable yarding operations. Eur J For Res 143, 1593–1609. https://doi.org/10.1007/s10342-024-01714-9

Marchi, L., Mologni, O., Trutalli, D., Scotta, R., Cavalli, R., Montecchio, L., Grigolato, S., (2019). Safety assessment of trees used as anchors in cable-supported tree harvesting based on experimental observations. Biosyst Eng 186, 71–82. https://doi.org/10.1016/j.biosystemseng.2019.06.022

Marchi, L., Trutalli, D., Mologni, O., Gallo, R., Roeser, D., Cavalli, R., Grigolato, S., (2021). Mechanical response of natural anchors in cable logging. International Journal of Forest Engineering 32, 29–42. https://doi.org/10.1080/14942119.2021.1826882

McPhearson, P. T. (2011). Toward a sustainable New York City: Greening through urban forest restoration. In *Sustainability in America's Cities: Creating the green metropolis* (pp. 181-203). Washington, DC: Island Press/Center for Resource Economics.

MEA - Millennium Ecosystem Assessment. Ecosystems and Human Well-being: Wetlands and Water. World Resources Institute (2005)

Moore, J.R., Maguire, D.A., (2004). Natural sway frequencies and damping ratios of trees: Concepts, review and synthesis of previous studies. Trees - Structure and Function 18, 195–203. https://doi.org/10.1007/s00468-003-0295-6

Nowak, D. J., Hirabayashi, S., Doyle, M., McGovern, M., & Pasher, J. (2018). Air pollution removal by urban forests in Canada and its effect on air quality and human health. Urban Forestry & Urban Greening, 29, 40-48.

Panalaran, S., & Sulisetyono, A. (2024). Pre-processing data and window function testing on wave spectrum analysis. In *IOP Conference Series: Earth and Environmental Science* (Vol. 1298, No. 1, p. 012037). IOP Publishing.

Schelhaas, M. J., Nabuurs, G. J., & Schuck, A. (2003). Natural disturbances in the European forests in the 19th and 20th centuries. *Global change biology*, *9*(11), 1620-1633.

Schindler, D., Fugmann, H., Schönborn, J., & Mayer, H. (2012). Coherent response of a group of plantation-grown Scots pine trees to wind loading. European Journal of Forest Research, 131(1), 191–202. https://doi.org/10.1007/s10342-010-0474-0

Schindler, D., & Mohr, M. (2018). Non-oscillatory response to wind loading dominates movement of Scots pine trees. Agricultural and Forest Meteorology, 250–251, 209–216. https://doi.org/10.1016/j.agrformet.2017.12.258

Schindler, D., & Mohr, M. (2019). No resonant response of Scots pine trees to wind excitation. Agricultural and Forest Meteorology, 265, 227–244. https://doi.org/ 10.1016/j.agrformet.2018.11.021

Schindler, D., Vogt, R., Fugmann, H., Rodriguez, M., Schönborn, J., & Mayer, H. (2010). Vibration behavior of plantation-grown Scots pine trees in response to wind excitation. Agricultural and Forest Meteorology, 150(7–8), 984–993. https://doi.org/10.1016/J.AGRFORMET.2010.03.003

Stoica, P., & Moses, R. L. (2005). *Spectral analysis of signals* (Vol. 452, pp. 25-26). Upper Saddle River, NJ: Pearson Prentice Hall.

van Haaften, M., Liu, Y., Wang, Y., Zhang, Y., Gardebroek, C., Heijman, W., & Meuwissen, M. (2021). Understanding tree failure—A systematic review and meta-analysis. *PloS one*, *16*(2), e0246805.

Woolsey, S. J. (2022). *Effects of Climate Change on the Probability of Urban Tree Failures from Wind Gusts* (Master's thesis, The University of Western Ontario (Canada)).

Young's modulus (modulus of elasticity) of wood. (n.d.). Amesweb.Info. Retrieved June 30, 2025, from https://amesweb.info/Materials/Youngs-Modulus-of-Wood.aspx

Zanotto, F., Grigolato, S., Schindler, D., Marchi, L., (2024a). Identifying wind-tree dynamics with numerical simulations based on experimental modal analysis. For Ecol Manage 569. https://doi.org/10.1016/J.FORECO.2024.122188

Zanotto, F., Kolbe, S., Stone, P., Grigolato, S., Schindler, D., & Marchi, L. (2025). A field comparison of sensor technologies to measure tree dynamics. *Computers and Electronics in Agriculture*. In press.

Zanotto, F., Marchi, L., & Grigolato, S. (2024b). Wind-tree interaction: Technologies, measurement systems for tree motion studies and future trends. *Biosystems Engineering*, *237*, 128–141. https://doi.org/10.1016/j.biosystemseng.2023.12.005